Applied Physics Letters

RESEARCH ARTICLE | MARCH 20 2024

Terahertz metallic waveguide with meta-holes for bidirectional conversion between two-dimensional guided waves and free-space waves

Tao Peng; Lei Zhang ; Ning Wang; Wei Chen ; Min Zhang ; Hong Su ; Ling Li ; Huawei Liang

Check for updates

Appl. Phys. Lett. 124, 121702 (2024)
https://doi.org/10.1063/5.0196667

View Online
Export Citation

31 August 2024 15:02:13

Nanotechnology & Materials Science
Optics & Photonics
Impedance Analysis
Scanning Probe Microscopy
Sensors
Failure Analysis & Semiconductors

Unlock the Full Spectrum.
From DC to 8.5 GHz.
Your Application. Measured.
Find out more
Zurich Instruments

AIP Publishing

Applied Physics Letters ARTICLE pubs.aip.org/aip/apl

Terahertz metallic waveguide with meta-holes for bidirectional conversion between two-dimensional guided waves and free-space waves

Cite as: Appl. Phys. Lett. **124**, 121702 (2024); doi: 10.1063/5.0196667
Submitted: 22 January 2024 · Accepted: 13 March 2024 ·
Published Online: 20 March 2024

View Online Export Citation CrossMark

Tao Peng,[1,2] Lei Zhang,[3] Ning Wang,[1,2] Wei Chen,[1,2] Min Zhang,[1,2] Hong Su,[1,2] Ling Li,[1,2] and Huawei Liang[1,2,a)]

AFFILIATIONS

[1]Key Laboratory of Optoelectronic Devices and Systems of Ministry of Education and Guangdong Province, Shenzhen University, Shenzhen 518060, People's Republic of China
[2]Shenzhen Key Laboratory of Laser Engineering, College of Physics and Optoelectronic Engineering, Shenzhen University, Shenzhen 518060, People's Republic of China
[3]Key Laboratory for Physical Electronics and Devices of the Ministry of Education and Shaanxi Key Lab of Information Photonic Technique, School of Electronic Science and Engineering, Xi'an Jiaotong University, Xi'an 710049, People's Republic of China

[a)]Author to whom correspondence should be addressed: hwliang@szu.edu.cn

31 August 2024 15:02:13

ABSTRACT

The conversion between guided and free-space waves is crucial for achieving integrated terahertz (THz) communication and signal processing. Herein, a bidirectional conversion mechanism is proposed for bridging two-dimensional (2D) guided waves and free-space waves, which is demonstrated by the wave manipulation of a metallic waveguide with meta-holes (MWMH). Compared with the conventional conversion between one-dimensional guided waves and free-space waves, in the proposed bidirectional conversion process, meta-holes can arbitrarily manipulate the phase of THz waves in higher dimensions, which enables stronger beam-manipulation capability and a higher gain. When used as a transmitting antenna, the MWMH exhibits excellent performance, i.e., a high gain (33.3 dBi), a high radiation efficiency (∼90%), and flexible beam manipulation. When the MWMH is reversely employed as a receiving antenna to obtain the focus of 2D guided waves, it achieves a gain of 27 dB and a focusing efficiency of 50.4%. The measured results for both the transmitting and receiving antennas agree well with the simulation results. The proposed bidirectional conversion mechanism facilitates the development of THz integrated photonic devices and is promising for application in the sixth-generation mobile communication, radar detection, and nondestructive testing.

Published under an exclusive license by AIP Publishing. https://doi.org/10.1063/5.0196667

Terahertz (THz) waves demonstrate significant application potential in many fields, such as the sixth-generation (6G) mobile communication, nondestructive testing, biomedicine, and integrated photonic devices.[1–4] However, compared with those of microwave and optical wave bands, the generation and detection technologies at the THz band are much more underdeveloped; thus, flexible THz control must be realized to compensate for these deficiencies.[5–7] Metasurfaces can be used to manipulate the amplitude, phase, and polarization of free-space waves[8–13] as well as to realize functions such as meta-lenses,[14,15] specific beam generation,[16,17] and meta-holograms,[18–20] which significantly benefit THz free-space manipulation. However, owing to the development of device integration and miniaturization, THz free-space manipulation no longer satisfies the requirements of on-chip signal processing and communication.[21] Thus, conversion control between THz guided waves and free-space waves is urgently required.[22,23]

In the THz band, spoof surface plasmon polariton metasurfaces are proposed to couple free-space waves to plasmonic and waveguide modes.[24–26] Conversely, some structures are proposed to realize the conversion from guided to free-space waves, such as plasmonic waveguides with chirped gratings, dielectric resonator antennas integrated with photonic crystal waveguides, leaky-wave antennas, and superheterodyne-inspired waveguide-integrated metasurfaces.[27–33] However, these structures were proposed primarily to realize coupling between one-dimensional (1D) guided waves (where the guided modes propagate along the longitudinal directions of waveguides and the phase on the waveguide cross section is identical) and free-space waves. Moreover, several 1D-control antennas have been integrated as

Published under an exclusive license by AIP Publishing

a planar array to attain a high gain or beam deflection in two orthogonal planes.[34,35] However, realizing the conversion between two-dimensional (2D) guided waves (where the propagation directions of the guided modes are unrestricted in the corresponding 2D plane and the phase on the waveguide cross section is typically unequal) and free-space waves remain challenging, particularly bidirectional conversion.

In this study, a bidirectional conversion mechanism is proposed for bridging 2D guided waves and free-space waves, which is demonstrated by the wave manipulation of a metallic waveguide with meta-holes (MWMH). Compared with conventional devices that only manipulate the conversion between 1D guided modes and free-space waves, meta-holes can arbitrarily manipulate the phase of THz waves in higher dimensions, which enables stronger beam-manipulation capability and higher gains. When used as a transmitting or receiving antenna, the MWMH exhibits excellent performance. The measured results have been shown to be consistent with simulation results.

Figure 1(a) shows the configuration of an MWMH, which comprises a rectangular parallel-plate metallic waveguide (PPMW) and an array of meta-holes engraved on one side. When the width of the PPMW, l, is much larger than the wavelength, λ, the reflection effect of guided waves on two boundaries perpendicular to the y-axis is typically negligible; thus, the PPMW can be regarded as infinitely wide. The propagation constant of the m-order transverse electric (TE) mode propagating in it can be calculated as follows:[36]

$$\beta_m = \sqrt{(n_0 k_0)^2 - \left(\frac{m\pi}{d}\right)^2}, \tag{1}$$

where $k_0 = \frac{2\pi}{\lambda}$; n_0 is the refractive index of air inside the waveguide, whose value is 1; and d is the plate separation. When $\frac{\lambda}{2} < d < \lambda$, only the TE_1 mode can be guided within the PPMW and its propagation constant is

$$\beta_1 = \sqrt{k_0^2 - \left(\frac{\pi}{d}\right)^2}. \tag{2}$$

This mode propagates along a straight line perpendicular to the waveguide cross section, on which the phases of the mode are identical. Thus, it can be regarded as a 1D guided mode. Under a frequency of $f = 0.14$ THz and a plate separation of $d = 2.1$ mm, the electric field distribution of the TE_1 mode is calculated using the commercial software COMSOL Multiphysics [see Fig. S1(a) in supplementary material]. Aluminum (Al) is adopted as the metal material, whose relative permittivity is described by the Drude model.[37] This mode propagates along the x-axis, and its field amplitude in the waveguide is constant along the y-axis. The propagation constant, β, remains unchanged for the waveguide width in the range of 0.1–45 mm [see Fig. S1(b)], which is consistent with Eq. (2).

In the THz band, obtaining a line radiation source with a width much larger than the wavelength for exciting the 1D TE mode is extremely challenging. When a frequently used sub-wavelength waveguide is adopted as the feed for the MWMH, the excited TE mode restricted along the z-axis direction propagates freely in the xy-plane and diverges in the form of a cylindrical wave with a finite height, as shown in Figs. 1(b) and 1(c). Thus, it differs from the TE_1 mode, which is called the 2D guided mode. The slight distortion of the wavefront near the boundaries perpendicular to the y-axis is caused by the boundary reflection, which minimally affects the propagation characteristics. The propagation constant is identical in the different propagation directions and can be determined using Eq. (2). Thus, the phase in the xy-plane can be written as

$$\varphi = \varphi_0 + \beta_1 R = \varphi_0 + \sqrt{k_0^2 - \left(\frac{\pi}{d}\right)^2} R, \tag{3}$$

where φ_0 is the phase on the output port of the waveguide feed and R is the distance of the cylindrical wave away from the feed. The phase and amplitude distributions of the 2D TE mode on the cross section +1 cm away from the feed are presented (see Fig. S2). None of the phases and amplitudes is constant along the y-axis, which differentiates the 2D guided mode from its 1D counterpart.

When the side lengths of the meta-hole cell, a and b, are both at the sub-wavelength scale, a TE_{10} mode can be excited in the meta-hole, and its electric-field distribution is presented in Fig. 2(a). It polarizes along the y-axis; thus, the y-polarized component of the 2D TE guided mode propagating in the PPMW can be coupled to the TE_{10}

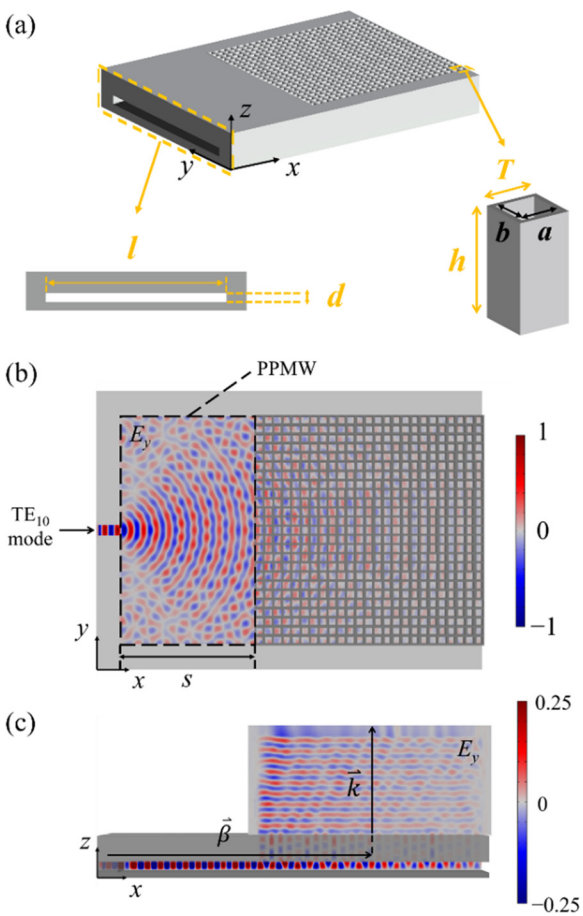

FIG. 1. THz MWMH for conversion from 2D guided waves to free-space waves. (a) Schematic illustration of MWMH. y-polarized electric field distributions in (b) xy- and (c) xz-planes.

31 August 2024 15:02:13

Published under an exclusive license by AIP Publishing

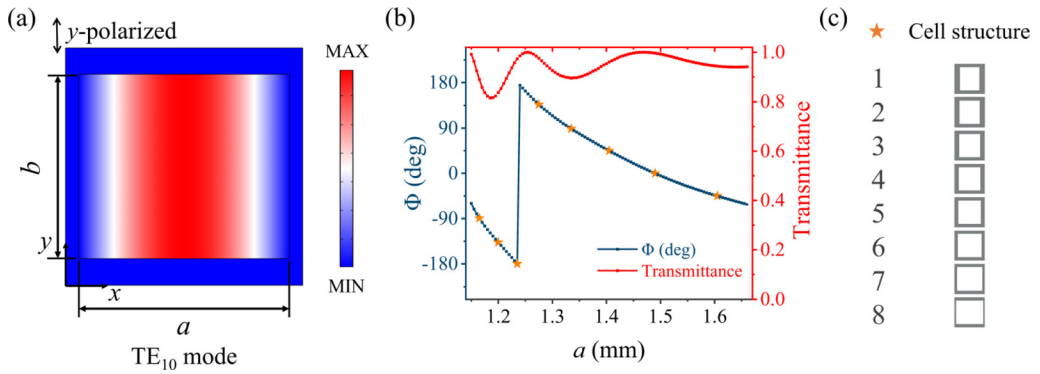

FIG. 2. (a) Electric field distribution of TE_{10} mode inside meta-hole cell. (b) Phase delay and intensity transmittance as functions of meta-hole side length *a*. (c) Cross-sectional patterns of selected eight meta-hole cells. Operating frequency $f = 0.14$ THz.

mode in the meta-hole. When the thickness of the meta-hole cell $h = 5$ mm, the period $T = 1.8$ mm, and the side length $b = 1.4$ mm, the phase delay and intensity transmittance as functions of the side length, *a*, for normal incidence are presented in Fig. 2(b). The entire range of phase control ($-180°$ to $180°$) can be achieved using the meta-holes, and the corresponding transmittance is extremely high owing to the extraordinary transmission effect.[38,39] Accordingly, eight cells were selected to encompass the phase range of $-180°$ to $180°$ with an interval of 45°, and their transmittances exceeded 80%. Their side lengths, *a*, were 1.165, 1.2, 1.235, 1.276, 1.333, 1.405, 1.49, and 1.605 mm, as shown in Fig. 2(c).

When the 2D TE guided mode arrives at the meta-holes, the phase at each location of the meta-hole array can be calculated using Eq. (3). By arranging the selected cells, some of the mode energy can be coupled into these meta-holes and the phase distribution on the output plane can be controlled simultaneously.[40] When the phase difference for the 2D guided mode at different locations is fully compensated by the phase control of these meta-holes, the 2D guided mode can be coupled into free space and the phases on the output plane are identical, as shown in Fig. 1(c). Consequently, the MWMH can achieve a complete conversion from a TE_{10} mode in the sub-wavelength waveguide feed to a 2D TE guided mode in the PPMW and then to a radiation mode in free space. For a single hole, the cell transmittance for the grazing incidence in this process is much lower than that for the normal incidence. However, most of the mode energy can be coupled into free space owing to scattering from numerous sub-wavelength meta-holes as well as the appropriate phase control. Compared with conventional devices, which only perform phase control in the 1D direction,[30] the MWMH can achieve arbitrary phase control in a 2D plane, which enables stronger beam-manipulation capability and higher gains.

To demonstrate the conversion from 2D guided waves to free-space waves, the MWMH was first employed as a THz transmitting antenna. The structure was optimized at $f = 0.14$ THz ($\lambda = 2.14$ mm). The cross-sectional dimensions of the meta-hole array were $21\lambda \times 21\lambda$. In the PPMW section, the width $l = 45$ mm and the length $s = 27$ mm. The height of the meta-hole cell $h = 5$ mm, and the plate separation $d = 2.1$ mm; thus, the antenna profile was ~ 7 mm. Moreover, the transmitting antenna is compatible with frequently used waveguide feeds, which allows their direct integration. When a rectangular waveguide with a cross section of $2.1 \times 2.1\ \mathrm{mm}^2$ was adopted as the feed, the MWMH successfully converted 2D guided waves to free-space waves as well as generated a high-gain radiating beam. The corresponding three-dimensional (3D) far-field radiation pattern is shown in Fig. 3(a), where θ is the elevation angle and φ is the azimuth angle. The antenna gain, *G*, can reach as high as 33.3 dBi, which is ~ 17 dB higher than that achieved by conventional THz leaky-wave antennas.[30] Figure 3(b) shows the radiation patterns in the H-plane (which comprises the magnetic-field vector and the direction of maximum radiation) and E-plane (which comprises the electric-field vector and the direction of maximum radiation). The 3-dB beamwidths of the mainlobe in the H- and E-planes were 2.6° and 2.8°, respectively, and the corresponding sidelobe levels were 10 and 15 dB lower than those of the mainlobe, respectively. The theoretical radiation efficiency of the entire model η (the ratio of the radiated power in the Fresnel diffraction region to the feed power) was up to 90%, as shown in Fig. 3(c). The 3-dB gain bandwidth spanned from 0.133 to 0.145 THz, which was restricted by the phase delays of both the metallic waveguide and meta-holes. The reflection coefficient was lower than -15 dB in the calculated range of 0.120–0.150 THz (see Fig. S3). Thus, even without a complex and costly feed network, the proposed MWMH can function as a high-gain, high-radiation-efficiency THz transmitting antenna with a low return loss.

The inclination angle of the equiphase plane can be adjusted by changing the arrangement of the meta-holes; thus, the radiation beam can be deflected in the plane with an arbitrary azimuthal angle. The beam deflections in the H-, and E-, and diagonal-planes are presented (see Figs. S4–S6), respectively, which differentiate the MWMH from conventional 1D-control leaky-wave antennas.[30,32,33] The gains remained extremely high for a deflection angle of 17°, and the 3-dB beamwidths of the main lobes were all $\sim 3°$.

Equation (2) indicates that the propagation constant of the TE mode depends on the operating frequency (wavelength) for a specified plate separation. Similarly, the phase-control characteristics of the meta-holes depend on the frequency. Thus, along with change in the frequency, the directional angle of the mainlobe deflects in the *xz*-plane and the gain decreases correspondingly, as shown in Fig. 3(d). Compared with the case at a center frequency of 0.14 THz, the deflection angles of the main lobes at frequencies of 0.135 and 0.145 THz were $+2.5°$ and $-2.5°$, respectively. Therefore, THz signals with

31 August 2024 15:02:13

Published under an exclusive license by AIP Publishing

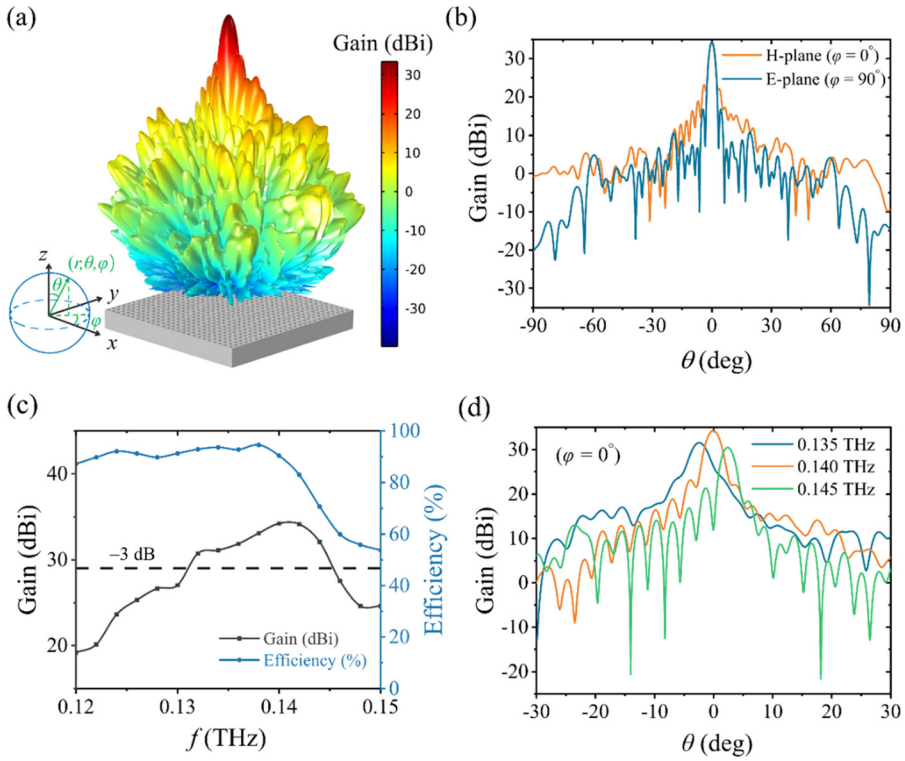

FIG. 3. MWMH used as THz transmitting antenna. (a) 3D radiation pattern. (b) Radiation patterns in H- and E-planes. (c) Dependence of antenna gain and radiation efficiency on frequency. (d) Radiation patterns in H-plane at frequencies of 0.135, 0.140, and 0.145 THz.

different frequencies can be detected in different directions, which are applicable to frequency division multiplexing technologies.[22,23]

Based on the design above, a prototype of the MWMH was fabricated using wire-cut electrical discharge machining (WEDM). Figure 4(a) shows the complete structure of the prototype, and Fig. 4(b) shows the top view of its two separated components. A schematic illustration and a physical photograph of the experimental setup for far-field measurements are presented [see Figs. S7(a) and S7(b)]. A

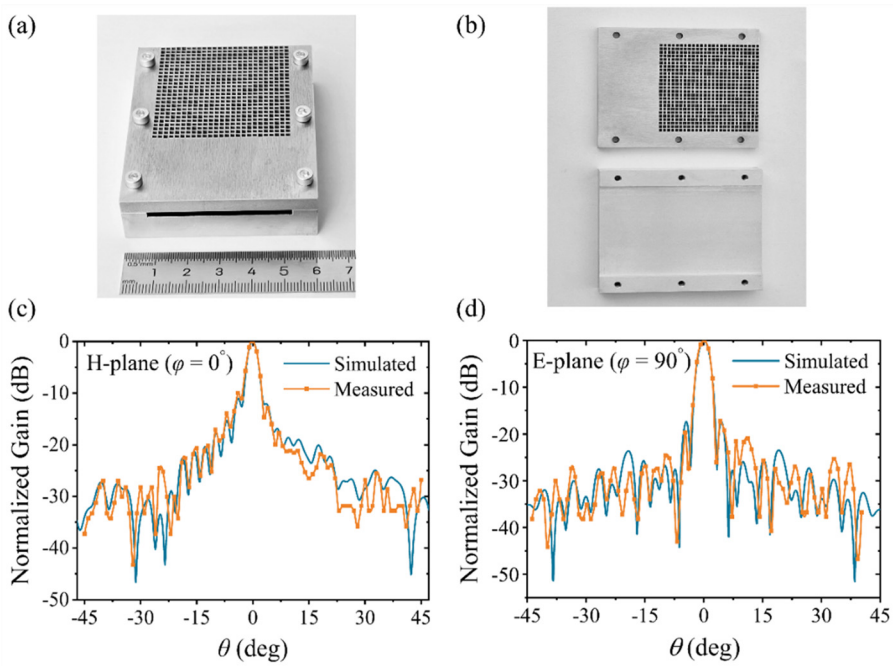

FIG. 4. (a) Fabricated prototype of THz MWMH. (b) Top view of its two separated components. Normalized radiation patterns in (c) H- and (d) E-planes. Operating frequency $f = 0.14$ THz.

31 August 2024 15:02:13

Published under an exclusive license by AIP Publishing

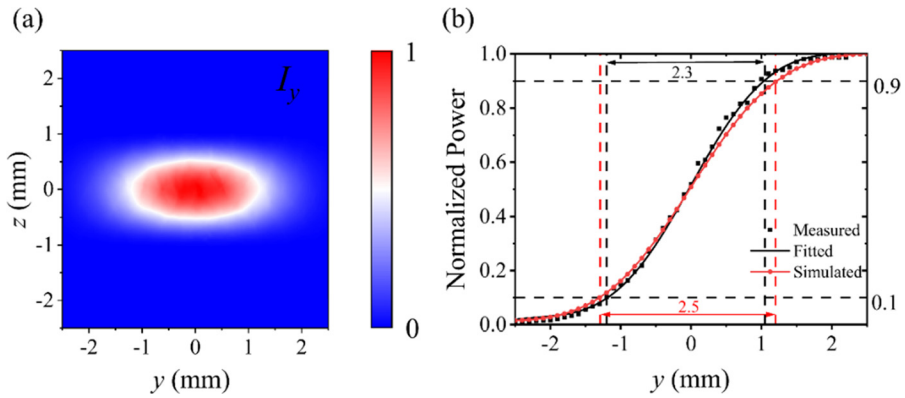

FIG. 5. MWMH used for focusing within PPMW. (a) Simulated electric field intensity distribution on focal plane. (b) Measured and simulated power curves on focal plane. Operating frequency $f = 0.14$ THz.

linearly polarized THz wave radiated from an impact-ionization avalanche crossing time (IMPATT) diode was coupled into the PPMW through a rectangular metallic waveguide, which was obtained from a metal baffle with a $2.1 \times 2.1\,\text{mm}^2$ hole and functioned as a feed. A THz power meter was employed for point-by-point measurements of the radiation intensity in the far field (1.9 m away from the MWMH prototype), which was shifted along an arc at an angle interval of 1°. The normalized radiation patterns in the H- and E-planes are shown in Figs. 4(c) and 4(d), respectively. The corresponding simulated results are presented as well for comparison, which agreed well with the measurements. When the elevation angle was extremely large, the simulated and measured curves deviated from each other, which was primarily caused by processing error and the measurement accuracy of the power meter. Recent experimental studies pertaining to THz transmitting antennas are summarized (see Table SI), which shows that the proposed MWMH offers the advantages of high gain, high radiation efficiency, and flexible beam manipulation.

Based on the electromagnetic reciprocity principle, the MWMH can be used as a THz receiving antenna by converting free-space waves into 2D guided waves. When y-polarized THz waves are normally incident on the meta-hole array, the y-polarized TE_{10} mode can be excited in each meta-hole and further coupled to the PPMW (see Fig. S8). The phase can be simultaneously manipulated using the meta-holes to compensate for the phase differences of the 2D guided waves propagating from different meta-holes to the target focus, which can be calculated using Eq. (3). Thus, the phases of the 2D guided waves originating from different meta-holes are identical at the focal point, and a focus caused by interference enhancement can be obtained in the PPMW. The field-intensity distribution on the focal plane is shown in Fig. 5(a). Compared with the incident wave, the gain at the focal point was up to 27 dB. The conversion efficiency (the ratio of the power on the focal plane to the input power) was 50.4%, which is comparable to the focusing efficiency of a commercial high density polyethylene lens.[41] In addition to the on-axis focusing above, the MWMH can realize more flexible wave control inside the PPMW, owing to the arbitrary phase control in the 2D plane. As an illustration, off-axis focusing was realized using the MWMH. On the focal plane, two spots were located ±1 cm away from the centerline along the y-axis, respectively [see Figs. S9(a) and S9(b)]. In contrast to lens focusing in free space, the MWMH can realize focusing in the waveguide by converting incident waves into cylindrical waves with sub-wavelength heights, which is preferred for the integration of THz photonic devices.

Based on the design above, an experimental setup was constructed to measure the spot width of the on-axis focusing. A schematic illustration and a physical photograph of the experimental setup are presented [see Figs. S10(a) and S10(b)]. The length of the PPMW in the prototype, s, was set to be equal to the focal length (27 mm), which is consistent with the length of the transmitting antenna, to facilitate the measurement of the spot width using the knife-edge method.[42] In the experiment, a linearly polarized THz wave radiating from an IMPATT diode was collimated using a commercial lens, and the collimated wave was coupled into the meta-hole array. By the phase control of the meta-holes, 2D guided waves were formed in the PPMW and further focused on the output port of the MWMH. A metal baffle was placed near the output port of the PPMW, and a THz power meter was used to measure the radiated power. The baffle was shifted point-by-point along the y-axis with a displacement accuracy of 100 μm, and the measured power is depicted in Fig. 5(b). The corresponding simulated results are presented as well for comparison. Based on the principle of the knife-edge method, the spot width along the y-axis is the coordinate difference, where the normalized powers are 0.1 and 0.9, respectively. Thus, the measured and simulated spot widths are 2.3 and 2.5 mm, respectively, which are numerically similar to each other. The small deviation is primarily caused by the reflection of the baffle edge and processing error. The spot width in the z-direction is smaller than 2.1 mm due to the confinement of the PPMW.

In summary, a bidirectional conversion mechanism was proposed to bridge the gap between 2D guided waves and free-space waves, as demonstrated by the wave manipulation of a MWMH. When the MWMH was employed as a transmitting antenna and integrated with a frequently used waveguide feed, it exhibited a high gain (33.3 dBi), a high radiation efficiency (90%), and flexible beam manipulation. When the MWMH was used as a receiving antenna to realize the conversion from free-space waves to 2D guided waves, the focusing gain was up to 27 dB, and the power on the focal plane was approximately 50.4% of the incident power. The bidirectional conversion mechanism, which combines waveguide technologies with metasurface-based wave control methods, facilitates the development of THz integrated sensing and communication and demonstrates significant application potential in 6G, radar detection, and nondestructive testing.

See the supplementary material for further detailed information about the 2D TE guided mode, the simulations of the flexible wave

31 August 2024 15:02:13

Published under an exclusive license by AIP Publishing

manipulation realized by the MWMH, and the schematics of experimental setups.

The authors thank the financial support provided by the National Natural Science Foundation of China under Grant No. 11874270; Natural Science Foundation of Guangdong Province, China under Grant Nos. 2022A1515011383 and 2022A1515011389; and Shenzhen Science and Technology Project under Grant No. JCYJ20200109105825504.

AUTHOR DECLARATIONS

Conflict of Interest

The authors have no conflicts to disclose.

Author Contributions

Tao Peng: Formal analysis (equal); Investigation (lead); Methodology (lead); Validation (equal); Writing – original draft (lead). **Lei Zhang:** Writing – review & editing (equal). **Ning Wang:** Investigation (equal). **Wei Chen:** Investigation (equal). **Min Zhang:** Resources (equal); Validation (equal). **Hong Su:** Resources (equal); Supervision (equal). **Ling Li:** Resources (equal); Validation (equal). **Huawei Liang:** Conceptualization (lead); Formal analysis (equal); Methodology (equal); Resources (lead); Supervision (lead); Validation (equal); Writing – review & editing (lead).

DATA AVAILABILITY

The data that support the findings of this study are available from the corresponding author upon reasonable request.

REFERENCES

[1]T. Nagatsuma, G. Ducournau, and C. C. Renaud, "Advances in terahertz communications accelerated by photonics," Nat. Photonics **10**, 371–379 (2016).
[2]S. Zhong, "Progress in terahertz nondestructive testing: A review," Front. Mech. Eng. **14**, 273–281 (2019).
[3]Y. Peng, C. Shi, Y. Zhu, M. Gu, and S. Zhuang, "Terahertz spectroscopy in biomedical field: A review on signal-to-noise ratio improvement," PhotoniX **1**, 12 (2020).
[4]S. Rajabali and I.-C. Benea-Chelmus, "Present and future of terahertz integrated photonic devices," APL Photonics **8**, 080901 (2023).
[5]B. Sensale-Rodriguez, R. Yan, M. M. Kelly, T. Fang, K. Tahy, W. S. Hwang, D. Jena, L. Liu, and H. G. Xing, "Broadband graphene terahertz modulators enabled by intraband transitions," Nat. Commun. **3**, 780 (2012).
[6]G. Liang, X. Hu, X. Yu, Y. Shen, L. H. Li, A. G. Davies, E. H. Linfield, H. K. Liang, Y. Zhang, S. F. Yu, and Q. J. Wang, "Integrated terahertz graphene modulator with 100% modulation depth," ACS Photonics **2**, 1559–1566 (2015).
[7]M. Mittendorff, S. Li, and T. E. Murphy, "Graphene-based waveguide-integrated terahertz modulator," ACS Photonics **4**, 316–321 (2017).
[8]N. Yu, P. Genevet, M. A. Kats, F. Aieta, J. P. Tetienne, F. Capasso, and Z. Gaburro, "Light propagation with phase discontinuities: Generalized laws of reflection and refraction," Science **334**, 333–337 (2011).
[9]A. Arbabi, Y. Horie, M. Bagheri, and A. Faraon, "Dielectric metasurfaces for complete control of phase and polarization with subwavelength spatial resolution and high transmission," Nat. Nanotechnol. **10**, 937–943 (2015).
[10]N. Yu and F. Capasso, "Flat optics with designer metasurfaces," Nat. Mater. **13**, 139–150 (2014).
[11]Z. Jiang, J. Lu, J. Fan, J. Liang, M. Zhang, H. Su, L. Zhang, and H. Liang, "Polarization-multiplexing Bessel vortex beams for polarization detection of continuous terahertz wave," Laser Photonics Rev. **17**, 2200484 (2023).
[12]A. Nemati, Q. Wang, M. Hong, and J. Teng, "Tunable and reconfigurable metasurfaces and metadevices," Opto-Electron. Adv. **1**, 180009 (2018).
[13]Z. Wang, S. Li, X. Zhang, X. Feng, Q. Wang, J. Han, Q. He, W. Zhang, S. Sun, and L. Zhou, "Excite spoof surface plasmons with tailored wavefronts using high-efficiency terahertz metasurfaces," Adv. Sci. **7**, 2000982 (2020).
[14]Q. Wang, X. Zhang, Y. Xu, Z. Tian, J. Gu, W. Yue, S. Zhang, J. Han, and W. Zhang, "A broadband metasurface-based terahertz flat-lens array," Adv. Opt. Mater. **3**, 779–785 (2015).
[15]H. Zhang, X. Zhang, Q. Xu, C. Tian, Q. Wang, Y. Xu, Y. Li, J. Gu, Z. Tian, C. Ouyang, X. Zhang, C. Hu, J. Han, and W. Zhang, "High-efficiency dielectric metasurfaces for polarization-dependent terahertz wavefront manipulation," Adv. Opt. Mater. **6**, 1700773 (2018).
[16]J. Liu, F. Fan, Z. Tan, H. Zhao, J. Cheng, and S. Chang, "Terahertz cascaded metasurfaces for both spin-symmetric and asymmetric beam diffractions with active power distribution," APL Photonics **8**, 096112 (2023).
[17]H. Zhang, X. Zhang, Q. Xu, Q. Wang, Y. Xu, M. Wei, Y. Li, J. Gu, Z. Tian, C. Ouyang, X. Zhang, C. Hu, J. Han, and W. Zhang, "Polarization-independent all-silicon dielectric metasurfaces in the terahertz regime," Photonics Res. **6**, 24–29 (2018).
[18]D. Hu, X.-K. Wang, S. Feng, J.-S. Ye, W.-F. Sun, Q. Kan, P. J. Klar, and Y. Zhang, "Ultrathin terahertz planar elements," Adv. Opt. Mater. **1**, 186–191 (2013).
[19]L. Huang, X. Chen, H. Mühlenbernd, H. Zhang, S. Chen, B. Bai, Q. Tan, G. Jin, K. W. Cheah, C.-W. Qiu, J. Li, T. Zentgraf, and S. Zhang, "Three-dimensional optical holography using a plasmonic metasurface," Nat. Commun. **4**, 2808 (2013).
[20]Q. Wang, E. Plum, Q. Yang, X. Zhang, Q. Xu, Y. Xu, J. Han, and W. Zhang, "Reflective chiral meta-holography: Multiplexing holograms for circularly polarized waves," Light: Sci. Appl. **7**, 25 (2018).
[21]G. Wu, J. Y. Dai, Q. Cheng, T. J. Cui, and C. H. Chan, "Sideband-free space-time-coding metasurface antennas," Nat. Electron. **5**, 808–819 (2022).
[22]N. Karl, R. W. McKinney, Y. Monnai, R. Mendis, and D. M. Mittleman, "Frequency-division multiplexing in the terahertz range using a leaky-wave antenna," Nat. Photonics **9**, 717–720 (2015).
[23]J. Ma, N. Karl, S. Bretin, G. Ducournau, and D. M. Mittleman, "Frequency-division multiplexer and demultiplexer for terahertz wireless links," Nat. Commun. **8**, 729 (2017).
[24]X. Zhang, Q. Xu, Q. Li, Y. Xu, J. Gu, Z. Tian, C. Ouyang, Y. Liu, S. Zhang, X. Zhang, J. Han, and W. Zhang, "Asymmetric excitation of surface plasmons by dark mode coupling," Sci. Adv. **2**, e1501142 (2016).
[25]Q. Xu, X. Zhang, Q. Yang, C. Tian, Y. Xu, J. Zhang, H. Zhao, Y. Li, C. Ouyang, Z. Tian, J. Gu, X. Zhang, J. Han, and W. Zhang, "Polarization-controlled asymmetric excitation of surface plasmons," Optica **4**, 1044–1051 (2017).
[26]Y. Zhang, Y. Xu, C. Tian, Q. Xu, X. Zhang, Y. Li, X. Zhang, J. Han, and W. Zhang, "Terahertz spoof surface-plasmon-polariton subwavelength waveguide," Photonics Res. **6**, 18–23 (2018).
[27]Y. Monnai, K. Altmann, C. Jansen, M. Koch, H. Hillmer, and H. Shinoda, "Terahertz beam focusing based on plasmonic waveguide scattering," Appl. Phys. Lett. **101**, 151116 (2012).
[28]W. Withayachumnankul, R. Yamada, C. Fumeaux, M. Fujita, and T. Nagatsuma, "All-dielectric integration of dielectric resonator antenna and photonic crystal waveguide," Opt. Express **25**, 14706–14714 (2017).
[29]H. Guerboukha, R. Shrestha, J. Neronha, O. Ryan, M. Hornbuckle, Z. Fang, and D. M. Mittleman, "Efficient leaky-wave antennas at terahertz frequencies generating highly directional beams," Appl. Phys. Lett. **117**, 261103 (2020).
[30]Q. L. Zhang, B. J. Chen, K. F. Chan, and C. H. Chan, "Terahertz circularly- and linearly polarized leaky-wave antennas based on spin-orbit interaction of spoof surface plasmon polaritons," IEEE Trans. Antennas Propag. **69**, 4347–4358 (2021).
[31]G. Wu, S. Zhu, S. W. Pang, and C. H. Chan, "Superheterodyne-inspired waveguide-integrated metasurfaces for flexible free-space light manipulation," Nanophotonics **11**, 4499–4514 (2022).
[32]K. Sarabandi, A. Jam, M. Vahidpour, and J. East, "A novel frequency beam-steering antenna array for submillimeter-wave applications," IEEE Trans. Terahertz Sci. Technol. **8**, 654–665 (2018).
[33]Y. W. Wu, Z. Jiang, and Z. C. Hao, "A 400-GHz low cost planar leaky-wave antenna with low sidelobe level and low cross-polarization level," IEEE Trans. Terahertz Sci. Technol. **10**, 427–430 (2020).

31 August 2024 15:02:13

Published under an exclusive license by AIP Publishing

[34]R. Camblor, S. V. Hoeye, M. Fernández, C. V. Antuña, and F. Las-Heras, "Full 2-D submillimeter-wave frequency scanning array," IEEE Trans. Antennas Propag. **65**, 4486–4494 (2017).
[35]S. S. Yao, Y. J. Cheng, Y. F. Wu, and H. N. Yang, "THz 2-D frequency scanning planar integrated array antenna with improved efficiency," Antennas Wirel. Propag. Lett. **20**, 983–987 (2021).
[36]D. M. Pozar, *Microwave Engineering*, 4th ed. (Wiley, New York, 2012).
[37]M. A. Ordal, R. J. Bell, R. W. Alexander, L. A. Newquist, and M. R. Querry, "Optical properties of Al, Fe, Ti, Ta, W, and Mo at submillimeter wavelengths," Appl. Opt. **27**, 1203–1209 (1988).
[38]T. W. Ebbesen, H. J. Lezec, H. F. Ghaemi, T. Thio, and P. A. Wolff, "Extraordinary optical transmission through sub-wavelength hole arrays," Nature **391**, 667–669 (1998).
[39]W. L. Barnes, A. Dereux, and T. W. Ebbesen, "Surface plasmon subwavelength optics," Nature **424**, 824–830 (2003).
[40]H. Liang, J. Li, Z. Wu, L. Zhang, and S. Ruan, "Metallic waveguide arrays for metasurface-like control with high simplicity in design," Adv. Opt. Mater. **8**, 2000605 (2020).
[41]J. Fan, L. Zhang, Z. Wu, J. Liang, T. Ning, M. Zhang, H. Su, and H. Liang, "Simultaneous and independent control of phase and polarization in terahertz band for functional integration of multiple devices," Opt. Laser Technol. **151**, 108064 (2022).
[42]Y. Suzaki and A. Tachibana, "Measurement of the μm sized radius of Gaussian laser beam using the scanning knife-edge," Appl. Opt. **14**, 2809–2810 (1975).

31 August 2024 15:02:13

Published under an exclusive license by AIP Publishing